EUROPEAN ORGANISATION FOR NUCLEAR RESEARCH (CERN)

CERN-EP-2024-051
February 26, 2024

K^0_S meson production in inelastic p+p interactions at 31, 40 and 80 GeV/c beam momentum measured by NA61/SHINE at the CERN SPS

The NA61/SHINE Collaboration

Measurements of K^0_S meson production via its $\pi^+\pi^-$ decay mode in inelastic p+p interactions at incident projectile momenta of 31, 40 and 80 GeV/c ($\sqrt{s_{NN}} = 7.7, 8.8$ and 12.3 GeV, respectively) are presented. The data were recorded by the NA61/SHINE spectrometer at the CERN Super Proton Synchrotron. Double-differential distributions were obtained in transverse momentum and rapidity. The mean multiplicities of K^0_S mesons were determined to be $(5.95 \pm 0.19(stat) \pm 0.22(sys)) \times 10^{-2}$ at 31 GeV/c, $(7.61 \pm 0.13(stat) \pm 0.31(sys)) \times 10^{-2}$ at 40 GeV/c and $(11.58 \pm 0.12(stat) \pm 0.37(sys)) \times 10^{-2}$ at 80 GeV/c. The results on K^0_S production are compared with model calculations (EPOS1.99, SMASH 2.0 and PHSD) as well as with published data from other experiments.

Contents

1 Introduction **4**

2 Experimental setup **5**

3 Analysis **6**
3.1 Data sets 6
3.2 Analysis method 7
3.3 Event selection 7
3.4 Track and topology selection 7
3.5 Raw K^0_S yields 8
3.6 Correction factors 9
3.7 Statistical uncertainties 11
3.8 Systematic uncertainties 12
3.9 Mean lifetime measurements 14

4 Results **15**
4.1 Transverse momentum spectra 15
4.2 Rapidity distributions and mean multiplicities 15

5 Comparison with published world data and model calculations **18**

6 Summary **23**

N. Abgrall[29], H. Adhikary[13], P. Adrich[15], K.K. Allison[26], N. Amin[5], E.V. Andronov[22], T. Antićić[3], I.-C. Arsene[12], M. Bajda[16], Y. Balkova[18], M. Baszczyk[17], D. Battaglia[25], A. Bazgir[13], S. Bhosale[14], M. Bielewicz[15], A. Blondel[4], M. Bogomilov[2], Y. Bondar[13], N. Bostan[25], A. Brandin[22], A. Bravar[29], W. Bryliński[21], J. Brzychczyk[16], M. Buryakov[22], A.F. Camino[28], M. Ćirković[23], M. Csanád[8], J. Cybowska[21], T. Czopowicz[13], C. Dalmazzone[4], N. Davis[14], A. Dmitriev[22], P. von Doetinchem[27], W. Dominik[19], P. Dorosz[17], J. Dumarchez[4], R. Engel[5], G.A. Feofilov[22], L. Fields[25], Z. Fodor[7,20], M. Friend[9], M. Gaździcki[13,6], O. Golosov[22], V. Golovatyuk[22], M. Golubeva[22], K. Grebieszkow[21], F. Guber[22], A. Haesler[29], S.N. Igolkin[22], S. Ilieva[2], A. Ivashkin[22], A. Izvestnyy[22], K. Kadija[3], N. Kargin[22], N. Karpushkin[22], E. Kashirin[22], M. Kiełbowicz[14], V.A. Kireyeu[22], H. Kitagawa[10], R. Kolesnikov[22], D. Kolev[2], A. Korzenev[29],Y. Koshio[10], V.N. Kovalenko[22], S. Kowalski[18], B. Kozłowski[21], A. Krasnoperov[22], W. Kucewicz[17], M. Kuchowicz[20], M. Kuich[19], A. Kurepin[22], A. László[7], M. Lewicki[20], G. Lykasov[22], V.V. Lyubushkin[22], M. Maćkowiak-Pawłowska[21], Z. Majka[16], A. Makhnev[22], B. Maksiak[15], A.I. Malakhov[22], A. Marcinek[14], A.D. Marino[26], H.-J. Mathes[5], T. Matulewicz[19], V. Matveev[22], G.L. Melkumov[22], A. Merzlaya[12], Ł. Mik[17], A. Morawiec[16], S. Morozov[22], Y. Nagai[8], T. Nakadaira[9], M. Naskręt[20], S. Nishimori[9], V. Ozvenchuk[14], O. Panova[13], V. Paolone[28], O. Petukhov[22], I. Pidhurskyi[13,6], R. Płaneta[16], P. Podlaski[19], B.A. Popov[22,4], B. Pórfy[7,8], M. Posiadała-Zezula[19], D.S. Prokhorova[22], D. Pszczel[15], S. Puławski[18], J. Puzović[23†], R. Renfordt[18], L. Ren[26], V.Z. Reyna Ortiz[13], D. Röhrich[11], E. Rondio[15], M. Roth[5], Ł. Rozpłochowski[14], B.T. Rumberger[26], M. Rumyantsev[22], A. Rustamov[1,6], M. Rybczynski[13], A. Rybicki[14], K. Sakashita[9], K. Schmidt[18], A.Yu. Seryakov[22], P. Seyboth[13], U.A. Shah[13], Y. Shiraishi[10], A. Shukla[27], M. Słodkowski[21], P. Staszel[16], G. Stefanek[13], J. Stepaniak[15], M. Strikhanov[22], H. Ströbele[6], T. Šuša[3], L. Swiderski[15], J. Szewiński[15], R. Szukiewicz[20], A. Taranenko[22], A. Tefelska[21], D. Tefelski[21], V. Tereshchenko[22], A. Toia[6], R. Tsenov[2], L. Turko[20], T.S. Tveter[12], M. Unger[5], M. Urbaniak[18], F.F. Valiev[22], D. Veberič[5], V.V. Vechernin[22], V. Volkov[22], A. Wickremasinghe[24], K. Wójcik[18], O. Wyszyński[13], A. Zaitsev[22], E.D. Zimmerman[26], A. Zviagina[22], and R. Zwaska[24]

† *deceased*

The NA61/SHINE Collaboration

[1] National Nuclear Research Center, Baku, Azerbaijan
[2] Faculty of Physics, University of Sofia, Sofia, Bulgaria
[3] Ruđer Bošković Institute, Zagreb, Croatia
[4] LPNHE, University of Paris VI and VII, Paris, France
[5] Karlsruhe Institute of Technology, Karlsruhe, Germany
[6] University of Frankfurt, Frankfurt, Germany
[7] Wigner Research Centre for Physics, Budapest, Hungary
[8] Eötvös Loránd University, Budapest, Hungary
[9] Institute for Particle and Nuclear Studies, Tsukuba, Japan
[10] Okayama University, Japan
[11] University of Bergen, Bergen, Norway
[12] University of Oslo, Oslo, Norway
[13] Jan Kochanowski University, Kielce, Poland
[14] Institute of Nuclear Physics, Polish Academy of Sciences, Cracow, Poland
[15] National Centre for Nuclear Research, Warsaw, Poland
[16] Jagiellonian University, Cracow, Poland
[17] AGH - University of Science and Technology, Cracow, Poland
[18] University of Silesia, Katowice, Poland

[19] University of Warsaw, Warsaw, Poland
[20] University of Wrocław, Wrocław, Poland
[21] Warsaw University of Technology, Warsaw, Poland
[22] Affiliated with an institution covered by a cooperation agreement with CERN
[23] University of Belgrade, Belgrade, Serbia
[24] Fermilab, Batavia, USA
[25] University of Notre Dame, Notre Dame, USA
[26] University of Colorado, Boulder, USA
[27] University of Hawaii at Manoa, Honolulu, USA
[28] University of Pittsburgh, Pittsburgh, USA
[29] University of Geneva, Geneva, Switzerland[1]

1 Introduction

The measurement of hadron production in proton-proton interactions plays a key role in understanding nucleus-nucleus collisions. In particular, it can shed some light on the creation process of Quark Gluon Plasma (QGP), on its properties, and on the characterization of the phase transition between hadronic matter and the QGP. One of the key signals of QGP creation is the enhanced production of s and $\bar{s}$ quarks, carried mostly by kaons [1]. The experimental results indicate that the creation of the QGP starts in nucleus-nucleus collisions at centre of mass energies from 10 to 20 GeV [2], which is the realm of the NA61/SHINE experiment at CERN. To explore this region systematically NA61/SHINE studies observables indicative of the QGP by a two-dimensional scan in collision energy and nuclear mass number of the colliding nuclei. Since 2009, NA61/SHINE has collected data on p+p, p+Pb, Be+Be, Ar+Sc, Xe+La and Pb+Pb interactions in the beam momentum range from 13A to 158A GeV/c [3]. Results on neutral kaon spectra in p+p at 158 GeV/c can be found in Ref. [4], while results on charged kaon spectra in p+p at 31, 40, 80 and 158 GeV/c can be found in Ref. [5]. In this paper, we present the results of K^0_S production in p+p collisions at 31, 40, and 80 GeV/c, which will be compared with K^0_S production at 158 GeV/c [4] and constitute the baseline for the interpretation of results obtained in heavier systems collected with the NA61/SHINE detector. Thanks to high statistics, large acceptance, and good momentum resolution the results presented here have, in general, higher precision than previously published measurements at SPS energies.

The paper is organised as follows. In Sec. 2, details of the NA61/SHINE detector system are presented. Section 3 is devoted to describing the analysis method. The results are shown in Sec. 4. In Sec. 5, they are compared to published world data and model calculations. Section 6 closes the paper with a summary and outlook.

The following units, variables and definitions are used in this paper. The particle mass and energy are presented in GeV, while particle momentum is shown in GeV/c. The particle rapidity y is calculated in the proton-proton collision center of mass system (cms), $y = 0.5 \cdot ln[(E + cp_L)/(E - cp_L)]$, where E and p_L are the particle energy and longitudinal momentum. The transverse component of the momentum is denoted as p_T. The momentum in the laboratory frame is denoted p_{lab} and the collision energy per nucleon pair in the centre of mass by $\sqrt{s_{NN}}$.

[1] No longer affiliated with the NA61/SHINE collaboration

2 Experimental setup

The NA61/SHINE collaboration uses a large acceptance spectrometer located in the CERN North Area. The schematic layout of the NA61/SHINE detector during the p+p data-taking is shown in Fig. 1. A detailed description of the experimental setup can be found in Ref. [6], while the details on the simulation in describing the detector performance across different kinematic variables as well as its inefficiencies can be found in Ref. [7].

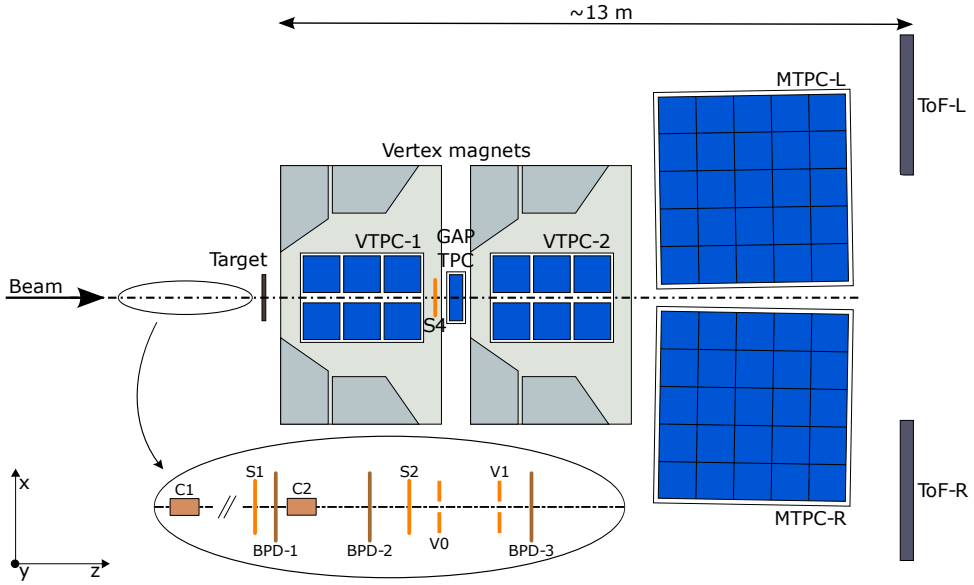

Figure 1: (Color online) The schematic layout of the NA61/SHINE experiment at the CERN SPS during p+p data taking (horizontal cut, not to scale). The beam and trigger detector configuration used for data taking in 2009 is shown in the inset (see Refs. [6–8] for a detailed description). The chosen coordinate system is drawn on the lower left: its origin lies in the middle of the VTPC-2 on the beam axis.

The main components of the NA61/SHINE spectrometer are four large-volume Time Projection Chambers (TPCs). Two of them, the vertex TPCs (VTPC-1 and VTPC-2), are located in the magnetic fields of two super-conducting dipole magnets with a maximum combined bending power of 9 Tm, which corresponds to about 1.5 T and 1.1 T in the upstream and downstream magnets, respectively. This field strength was used for data taking at 158 GeV/c and scaled down in proportion to the lower beam momenta to obtain similar $y - p_T$ acceptance at all beam momenta. Two large main TPCs (MTPC-L and MTPC-R) and two walls of pixel Time-of-Flight (ToF-L/R) detectors are positioned symmetrically to the beamline downstream of the magnets. A GAP-TPC (GTPC) is placed between VTPC-1 and VTPC-2 directly on the beamline. It closes the gap between the beam axis and the sensitive volumes of the other TPCs. The TPCs are filled with Ar and CO_2 gas mixtures in proportions 90:10 for the VTPCs and 95:5 for the MTPCs. Particle identification in the TPCs is based on measurements of the specific energy loss (dE/dx) in the chamber gas. Typical values for the momentum resolution are $\sigma(p)/p^2 = 7 \times 10^{-4}$ (GeV/c)$^{-1}$ for low-momentum tracks measured only in VTPC-1 ($p \leq 8$ GeV/c) and 3×10^{-3} (GeV/c)$^{-1}$ for tracks traversing the full detector up to and including the MTPCs ($p \geq 8$ GeV/c).

Secondary beams of positively charged hadrons at momenta of 31, 40 and 80 GeV/c were used to collect the data for the analysis presented in this paper. These beams were produced from a 400 GeV/c proton

beam extracted from the SPS in a slow extraction mode with a flat-top of 10 seconds. The beam momentum and intensity were adjusted by appropriate settings of the H2 beam line magnet currents and collimators. Protons from the secondary hadron beam are identified by two Cherenkov counters, C1 [9] and C2 (THC). The C1 counter, using a coincidence of six out of the eight photomultipliers placed radially along the Cherenkov ring, provides identification of protons, while the THC, operated at a pressure lower than the proton threshold, is used in anti-coincidence in the trigger logic. A selection based on the signals from the Cherenkov counters allowed to identify beam protons with a purity of about 99%, as demonstrated by a measurement of the specific ionization energy loss $\mathrm{d}E/\mathrm{d}x$ of the beam particles by bending the 31 GeV/c beam into the TPCs using the full magnetic field strength [10]. A set of scintillation (S1, S2 and V0, V1) and beam position detectors (BPDs) upstream of the spectrometer provide timing reference, and position measurements of incoming beam particles. The trigger scintillation counter S4 placed downstream of the target has a diameter of 2 cm. It is used to trigger the readout whenever an incoming beam particle, which is registered upstream of the target, does not hit S4, which indicates that an interaction occurred in the target area.

A cylindrical target vessel of 20.29 cm length and 3 cm diameter was placed upstream of the entrance window of VTPC-1 (center of the target is at z = -581 cm in the NA61/SHINE coordinate system). The vessel was filled with liquid hydrogen corresponding to an interaction length of 2.8%. The liquid hydrogen had a density of approximately 0.07 g/cm^3. Data were taken with the vessel filled with liquid hydrogen and being empty. Here, only events recorded with the target vessel filled with hydrogen were analyzed.

3 Analysis

3.1 Data sets

The presented results on K^0_S production in inelastic p+p interactions at $p_{beam} = 31, 40$ and 80 GeV/c are based on data recorded in 2009. Table 1 summarizes basic information about data sets used in the analysis, the number of events selected by interaction trigger and the number of events after analysis cuts. The event numbers recorded with the interaction trigger were 2.85M, 4.37M and 3.80M, respectively. The drop in event numbers after cuts is caused mainly by BPD reconstruction inefficiencies and off-target interactions accepted by the trigger logic.

p_{beam} (GeV/c)	$\sqrt{s_{NN}}$ (GeV)	Number of recorded events with interaction trigger	Number of events after selection criteria
31	7.7	2.85×10^6	0.83×10^6
40	8.8	4.37×10^6	1.24×10^6
80	12.3	3.80×10^6	1.48×10^6

Table 1: Data sets used for the analysis of K^0_S production. The beam momentum is denoted by p_{beam}, whereas $\sqrt{s_{NN}}$ is the energy available in the center-of-mass system for the nucleon pair. The events selection criteria are described in Sec. 3.3.

3.2 Analysis method

The event vertex and the produced particle tracks were reconstructed using the standard NA61/SHINE software. Details of the track and vertex reconstruction procedures can be found in Refs. [7, 8, 11]. Detector parameters were optimized by a data-based calibration procedure, which also considered their time dependence; for details, see Refs. [5, 12]. The following section enumerates the criteria for selecting events, tracks and the K_S^0 decay topology. Then, the simulation-based correction procedure is described and used to quantify the losses due to reconstruction inefficiencies and limited geometrical acceptance.

3.3 Event selection

The criteria for selection of inelastic p+p interactions are the following:

(i) An event was accepted by the trigger logic (see Refs. [7, 8]) as an interaction candidate event.

(ii) No off-time beam particle was detected within a time window of ± 2 μs around the trigger particle.

(iii) Beam particle trajectory was measured in at least three planes out of four of BPD-1 and BPD-2 and in both planes of BPD-3.

(iv) The primary interaction vertex fit converged.

(v) The z position of the interaction vertex (fitted using the beam trajectory and TPC tracks) not farther away than 9 cm from the center of the target vessel.

(vi) Events with a single, well-measured, positively charged track with absolute momentum close to the beam momentum ($p > p_{beam} - 1$ GeV/c) were rejected.

The background due to elastic interactions was removed via cuts (iv) and (vi). The contribution from off-target interactions was reduced by cut (v). The simulations corrected the losses of inelastic p+p interactions due to the event selection procedure.

The numbers of events left after the selection criteria described in the text above are given in Table 1.

3.4 Track and topology selection

Neutral strange particles are detected and measured using their weak decay into charged particles. The K_S^0 decays into $\pi^+ + \pi^-$ with a branching ratio of 69.2% [13] are used here. The decay particles form the so-called V^0 topology. K_S^0 decay candidates (V^0s) are obtained by pairing all positively with all negatively charged pion candidates. The tracks of the decay pions and the V^0 topology are subject to the following additional selection criteria:

(i) For each candidate track, the minimum number of measured clusters in VTPC-1 and VTPC-2 must be 15.

(ii) All pion tracks must have a measured specific energy loss ($\mathrm{d}E/\mathrm{d}x$) in the TPCs within $\pm 3\sigma$ around the nominal Bethe-Bloch value for charged pions. Here, σ represents the typical standard deviation of a Gaussian fitted to the $\mathrm{d}E/\mathrm{d}x$ distribution of pions. Since only small variations of σ were observed for different bins and beam momenta, a constant value $\sigma = 0.052$ is used [14]. This selection criterion applies only to experimental data, not MC-simulated events (see below).

(iii) The distance |Δz| between the z-coordinates of the primary production and the K^0_S decay vertices is required to lie in the rapidity dependent range: $|\Delta z| > e^{a+b\cdot y_{lab}}$, with y_{lab} the rapidity in the laboratory and a and b constants which amount to 1.91 and 0.99 for the $p_{beam} = 31$ GeV/c, 1.71 and 0.95 for $p_{beam} = 40$ GeV/c, and 1.85 and 0.90 for $p_{beam} = 80$ GeV/c data sets, respectively.

(iv) The distance of closest approach (DCA) in the x and y directions of the straight line given by the K^0_S momentum vector in the laboratory and the primary vertex must be smaller than 0.25 cm, with DCA given by $\sqrt{(b_x/2)^2 + {b_y}^2}$.

(v) The cosine of the angle between the V^0 and π^+ momentum vectors in the K^0_S rest frame has to be in the range: $-0.97 < cos\Theta^* < 0.85$.

The quality of the aforementioned track and topology selection criteria is illustrated in Fig. 2. The population of K^0_S decay candidates is shown as a function of the two Armenteros-Podolansky variables p_T^{Arm} and α^{Arm} [15] and after all track and topology selection criteria. The quantity p_T^{Arm} is the transverse momentum of the decay particles with respect to the direction of motion of the V^0 candidate and $\alpha^{Arm} = (p_L^+ - p_L^-)/(p_L^+ + p_L^-)$, where p_L^+ and p_L^- are the longitudinal momenta of the positively and negatively charged V^0 daughter particles, measured with respect to the V^0's direction of motion. From the plots (see Fig. 2) one can see that contributions of Λ and $\bar{\Lambda}$ hyperons are removed by the topological selection criteria.

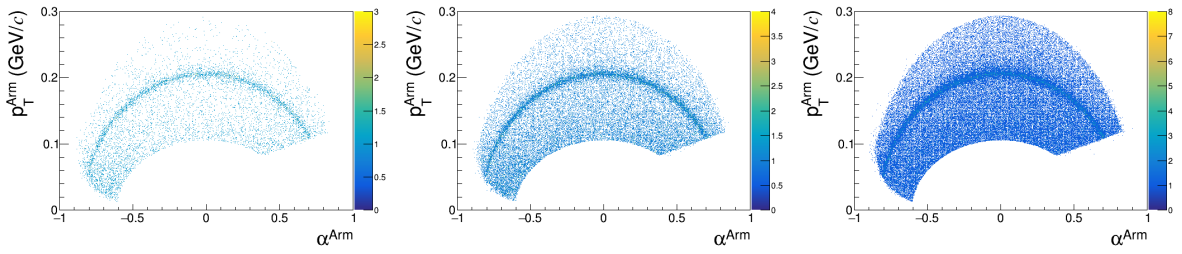

Figure 2: Armenteros-Podolanski plots of V^0 candidates after all track and topology selection criteria for $p_{beam} = 31, 40$ and 80 GeV/c from left to right. The boundaries on the plots' left and right sides result from using the $cos\Theta^*$ cut, while the upper and lower boundaries are shaped by selecting a certain invariant mass range.

3.5 Raw K^0_S yields

The double differential uncorrected yields of K^0_S are determined by studying the invariant mass distributions of the accepted pion pairs in bins of rapidity and transverse momentum (examples are presented in Fig. 3). The K^0_S decays will appear as a peak over a smooth combinatorial background. The K^0_S yield was determined in each bin using a fit function that describes both the signal and the background. A Lorentzian function was used for the signal:

$$L(m) = A\frac{1}{\pi}\frac{\frac{1}{2}\Gamma}{(m-m_0)^2 + (\frac{1}{2}\Gamma)^2}\ , \tag{1}$$

where A is the normalization factor, Γ is the full width at half maximum of the signal peak, and m_0 is the mass parameter. The background contribution is described by a polynomial function of 2^{nd} order.

Figure 3 shows examples of $\pi^+\pi^-$ invariant mass distributions obtained from the $p_{beam} = 40$ GeV/c data set after all V^0 selection cuts for real data (*left*) and for simulated events (*right*).

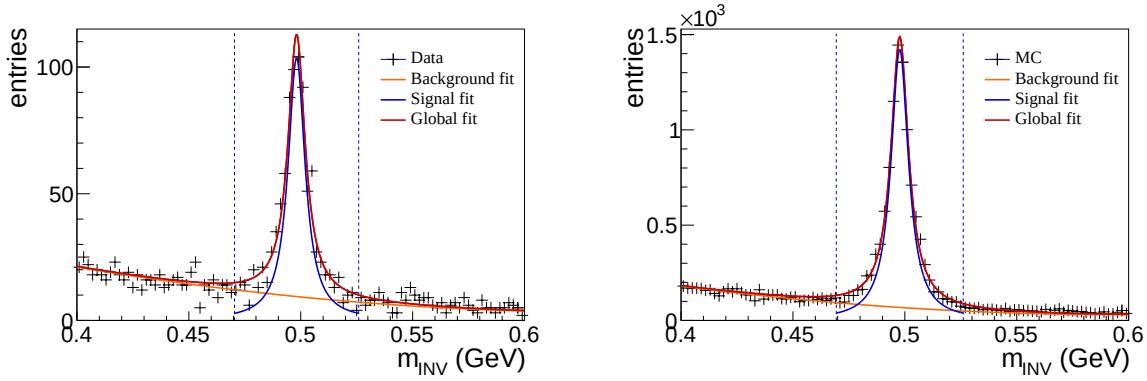

Figure 3: The invariant mass distribution of K^0_S candidates for experimental data (*left*) and MC (*right*) for the $p_{beam} = 40$ GeV/c data set for $-0.25 \leq y < 0.25$ and $0.2 \leq p_T < 0.4$ after all selection criteria. The dashed-blue vertical lines indicate the regions where the K^0_S signal was integrated. The signal data points are black, the fitted background is orange, the fitted signal is blue, and the total fit results are red. Mass resolutions obtained from the fits are: $\sigma = (0.00925 \pm 0.00064)$ GeV for the experimental data and $\sigma = (0.00946 \pm 0.00017)$ GeV for the MC.

The procedure of fitting the histograms proceeds in three steps. In the first step, the background outside the signal peak ([0.475-0.525] GeV) is fitted with a polynomial of 2^{nd} order. This step is necessary to obtain starting values for the parameters of the background function. In the next step, a full invariant mass spectrum fit is performed with the sum of the Lorentzian and the background function. The initial parameter values for the background function are taken from the previous step, the mass parameter is fixed to the PDG value of $m_0 = 0.497614(24)$ GeV [13], and the width is allowed to vary between 0.005 and 0.03 GeV. Finally, in the last step, all parameters are free, and the fitting region is [0.35-0.65] GeV. The orange and blue curves in Fig. 3 show the fitted polynomial background and the Lorentzian signal function. To minimize the sensitivity of the K^0_S yield to the integration window, the uncorrected number of K^0_S was calculated by subtracting bin-by-bin the fitted background (B) and summing the background-subtracted signal in the mass window $m_0 \pm 3\Gamma$ (dashed vertical lines), where m_0 is the fitted mass of the K^0_S. Figure 3 shows that the simulation reproduces the central value of the K^0_S mass distribution and its width agree with the data within uncertainties. The Γ parameter fitted to the simulation was used to calculate the signal from the simulation. Thus, a possible bias due to differences between the data and the simulation is reduced; see Sec. 3.8.

The uncorrected bin-by-bin K^0_S multiplicities and their statistical uncertainties are shown in Fig. 4.

3.6 Correction factors

A correction for interactions of the incident protons with the target vessel is not needed, because the distributions of the primary vertex coordinates show no sign of such events after the event and track selection cuts. A detailed Monte Carlo simulation was performed to compute the corrections for losses due to the trigger bias, geometrical acceptance, reconstruction efficiency, and the selection criteria applied in the analysis. The correction factors are based on 20×10^6 inelastic p+p events at each beam momenta

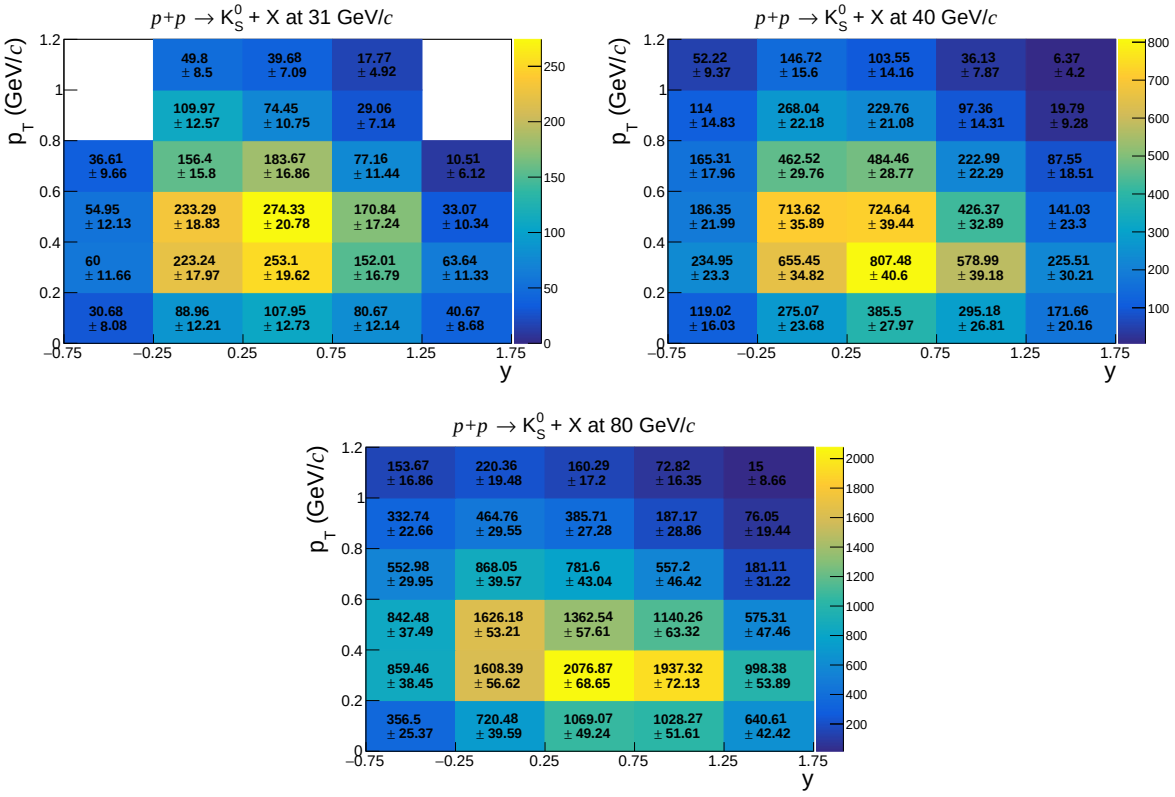

Figure 4: Uncorrected bin-by-bin multiplicities of K^0_S with their statistical uncertainties for $p_{beam} = 31$ GeV/c (*left*), $p_{beam} = 40$ GeV/c (*right*) and $p_{beam} = 80$ GeV/c (*bottom*).

$p_{beam} = 31, 40$ and 80 GeV/c produced by the EPOS1.99 event generator [16, 17]. Particles in the generated events were tracked through the NA61/SHINE apparatus using the GEANT3 package [18]. The TPC response was simulated by dedicated software packages that account for known detector effects. The simulated events were reconstructed with the same software as the real events, and the same selection cuts were applied. However, $\mathrm{d}E/\mathrm{d}x$ identification was replaced by matching reconstructed tracks to simulated ones. The branching ratio of K^0_S decays is taken into account in the GEANT3 software package. For each y and p_T bin, the correction factor $c_{MC}(y, p_T)$ was calculated as:

$$c_{MC}(y, p_T) = \frac{n^{gen}_{MC}(y, p_T)}{N^{gen}_{MC}} \Big/ \frac{n^{acc}_{MC}(y, p_T)}{N^{acc}_{MC}} , \tag{2}$$

where:

- $n^{gen}_{MC}(y, p_T)$ is the number of K^0_S generated in a given (y, p_T) bin,
- $n^{acc}_{MC}(y, p_T)$ is the number of reconstructed K^0_S in a given (y, p_T) bin.
- N^{gen}_{MC} is the number of generated inelastic p+p interactions (20×10^6),
- N^{acc}_{MC} is the number of accepted p+p events (about 13.5×10^6 for all three beam momenta).

The loss of the K^0_S mesons due to the $\mathrm{d}E/\mathrm{d}x$ cut is corrected with an additional factor:

$$c_{dE/dx} = \frac{1}{\varepsilon^2} = 1.005 \ , \tag{3}$$

where $\varepsilon = 0.9973$ is the probability for the pions to be detected within $\pm 3\sigma$ around the nominal Bethe-Bloch value.

The double-differential yield of K^0_S per inelastic event in bins of (y, p_T) is calculated as follows:

$$\frac{d^2n}{dy\,dp_T}(y, p_T) = \frac{c_{dE/dx} \cdot c_{MC}(y, p_T)}{\Delta y \Delta p_T} \cdot \frac{n_{K^0_S}(y, p_T)}{N_{events}} \ , \tag{4}$$

where:

- $c_{dE/dx}$, $c_{MC}(y, p_T)$ are the correction factors described above,
- Δy and Δp_T are the bin widths,
- $n_{K^0_S}(y, p_T)$ is the uncorrected number of K^0_S , obtained by the signal extraction procedure described in Sec. 3.5. The corresponding values are presented in Fig. 4,
- N_{events} is the number of events left in the sample after selection criteria.

3.7 Statistical uncertainties

The statistical uncertainties of the corrected double-differential yields (see Eq. 4) receive contributions from the statistical uncertainty of the correction factor $c_{MC}(y, p_T)$ and the statistical uncertainty of the uncorrected number of K^0_S ($\Delta N_{K^0_S}(y, p_T)$). The statistical uncertainty of the former receives two contributions, the first, α, caused by the loss of inelastic interactions due to the event selection and the second, β, connected with the loss of K^0_S candidates due to the V^0 selection:

$$c_{MC}(y, p_T) = \frac{n^{gen}_{MC}(y, p_T)}{N^{gen}_{MC}} \Big/ \frac{n^{acc}_{MC}(y, p_T)}{N^{acc}_{MC}} = \frac{N^{acc}_{MC}}{N^{gen}_{MC}} \Big/ \frac{n^{acc}_{MC}(y, p_T)}{n^{gen}_{MC}(y, p_T)} = \frac{\alpha}{\beta(y, p_T)} \ , \tag{5}$$

The error of α is calculated assuming a binomial distribution:

$$\Delta\alpha = \sqrt{\frac{\alpha(1-\alpha)}{N^{gen}_{MC}}} \ , \tag{6}$$

The error of β is calculated according to the formula:

$$\Delta\beta(y, p_T) = \sqrt{\left(\frac{\Delta n^{acc}_{MC}(y, p_T)}{n^{gen}_{MC}(y, p_T)}\right)^2 + \left(\frac{n^{acc}_{MC}(y, p_T) \cdot \Delta n^{gen}_{MC}(y, p_T)}{(n^{gen}_{MC}(y, p_T))^2}\right)^2} \ , \tag{7}$$

where $\Delta n^{acc}_{MC}(y, p_T) = \sqrt{S + B}$ see Sec. 3.5, and $\Delta n^{gen}_{MC}(y, p_T) = \sqrt{n^{gen}_{MC}(y, p_T)}$. The equation for $\Delta c_{MC}(y, p_T)$ can be written as:

$$\Delta c_{MC}(y,p_T) = \sqrt{\left(\frac{\Delta\alpha}{\beta}\right)^2 + \left(-\frac{\alpha\cdot\Delta\beta}{\beta^2}\right)^2}\,. \tag{8}$$

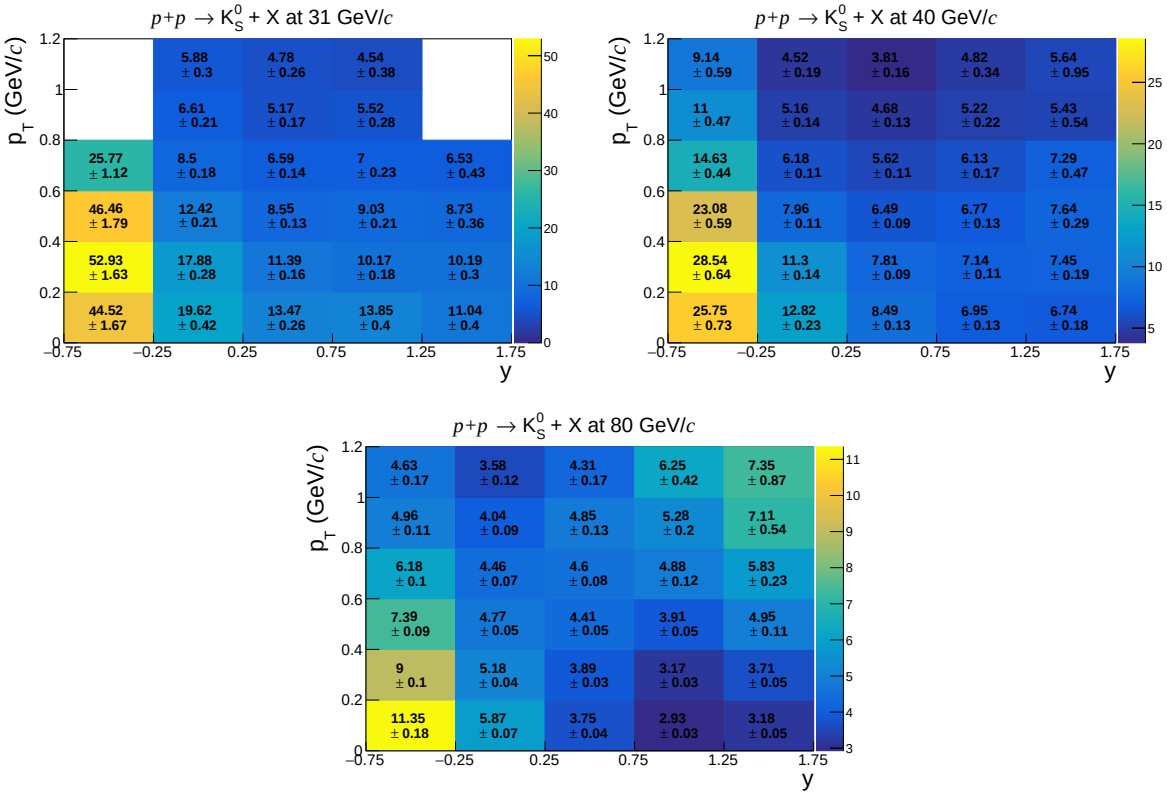

Figure 5: Monte-Carlo correction factors (see Eq. 2) with their statistical uncertainties (see Eq. 8) in each (y, p_T) bin for $p_{beam} = 31$ GeV/c (*left*), $p_{beam} = 40$ GeV/c (*right*) and $p_{beam} = 80$ GeV/c (*bottom*).

Finally, the statistical uncertainties $\Delta n_{K^0_S}(y,p_T)$ of the corrected number of K^0_S are:

$$\Delta\frac{d^2n}{dydp_T}(y,p_T) = \sqrt{\left(\frac{c_{dE/dx}\cdot c_{MC}(y,p_T)}{N_{events}\Delta y\Delta p_T}\right)^2 \Delta n^2_{K^0_S}(y,p_T) + \left(\frac{c_{dE/dx}\cdot n_{K^0_S}(y,p_T)}{N_{events}\Delta y\Delta p_T}\right)^2 \Delta c^2_{MC}(y,p_T)}\,. \tag{9}$$

3.8 Systematic uncertainties

Three possible contributions to the systematic uncertainties related to the event selection criteria, the track and V^0 selection criteria and the signal extraction procedure were considered.

(i) The uncertainties related to the event selection criteria (see Sec. 3.3) were estimated by performing the analysis with the following changes:

- Simulations were done with and without the S4 trigger condition for all inelastic p+p interactions. One-half of the difference between these two results was taken as the contribution to the systematic uncertainty, which amounts to up to 3%.
- The allowed range of the vertex z position was changed from -590 < z (cm) < -572 to -588 < z (cm) < -574 and -592 < z (cm) < -570. The uncertainty due to the variation of the selection window amounts to up to 4%.

(ii) The uncertainties related to the track and V^0 selection criteria were estimated by performing the analysis with the following changes compared to the original values (see Sec. 3.4):

- the minimum required number of clusters in both VTPCs for V^0 daughters was changed from 15 to 12 and 18, indicating a possible bias of up to 2%,
- the standard $\mathrm{d}E/\mathrm{d}x$ cut used for identification of V^0 daughters was changed from $\pm 3\sigma$ to $\pm 2.5\sigma$ and $\pm 3.5\sigma$ from the nominal Bethe-Bloch value indicating a possible bias of up to 3%,
- the Δz cut was changed by varying the parameters a and b from 1.91 to 2.01 and 1.81 for parameter a and from 0.99 to 0.98 and 1.00 for parameter b for $p_{beam} = 31$ GeV/c, from 1.71 to 1.91 and 1.51 for parameter a and from 0.95 to 0.93 and 0.97 for parameter b for $p_{beam} = 40$ GeV/c and from 1.85 to 2.05 and 1.65 for parameter a and from 0.90 to 0.88 and 0.92 for parameter b for $p_{beam} = 80$ GeV/c, indicating a possible bias of up to 2%,
- the allowed distance of closest approach of the K^0_S trajectory to the primary vertex was varied from 0.25 to 0.20 and 0.30 cm, indicating a possible bias of up to 3%,
- the $cos\Theta^*$ range for accepted candidates was changed from $-0.97 < cos\Theta^* < 0.85$ to $-0.99 < cos\Theta^* < 0.87$ and $-0.95 < cos\Theta^* < 0.83$ indicating a possible bias of up to 3%.

(iii) The uncertainty due to the signal extraction procedure (see Sec. 3.5) was estimated by:

- changing the background fit function from a 2^{nd} order to a 3^{rd} order polynomial indicating a possible bias of up to 4%,
- changing the invariant mass range over which the uncorrected number of K^0_S was integrated from $m_0 \pm 3\Gamma$ to $m_0 \pm 2.5\Gamma$ and $m_0 \pm 3.5\Gamma$ indicating a possible bias of up to 2%,
- calculating the uncorrected number of K^0_S as the sum of entries after background fit subtraction instead of the integral of the Lorentzian signal function indicating a possible bias of up to 2%,
- changing the region of the fit from [0.35-0.65] GeV/c^2 to [0.38-0.62] GeV/c^2 indicating a possible bias of up to 2%.

The maximum deviations are determined separately for each group of contributions to the systematic uncertainty. The systematic uncertainty was calculated as the square root of the sum of squares of the maximum deviations. This procedure was used to estimate systematic uncertainties of all final quantities presented in this paper: yields in (y, p_T) bins, inverse slope parameters of transverse momentum spectra, yields in rapidity bins, and mean multiplicities.

3.9 Mean lifetime measurements

The reliability of the K^0_S reconstruction and the correction procedure was validated by studying the lifetime distribution of the analyzed K^0_S . The lifetime ($c\tau$) of each identified K^0_S was calculated from the V^0 path length and its velocity. The corrected number of K^0_S was then determined in bins of $c\tau/c\tau_{PDG}$, and for the five rapidity bins of the $p_{beam} = 40$ GeV/c and 80 GeV/c data sets and in the whole rapidity range ($-0.75 < y < 1.75$) of the $p_{beam} = 31$ GeV/c data set (see Fig. 6). The straight lines in Fig. 6 represent the results of exponential fits, which provide mean lifetime values (normalized to the known PDG value [13]) as a function of rapidity. The thus determined mean lifetimes are shown in Fig. 7 as a function of rapidity. The measured mean K^0_S lifetimes agree within uncertainties with the PDG value and thus confirm the quality of the analysis.

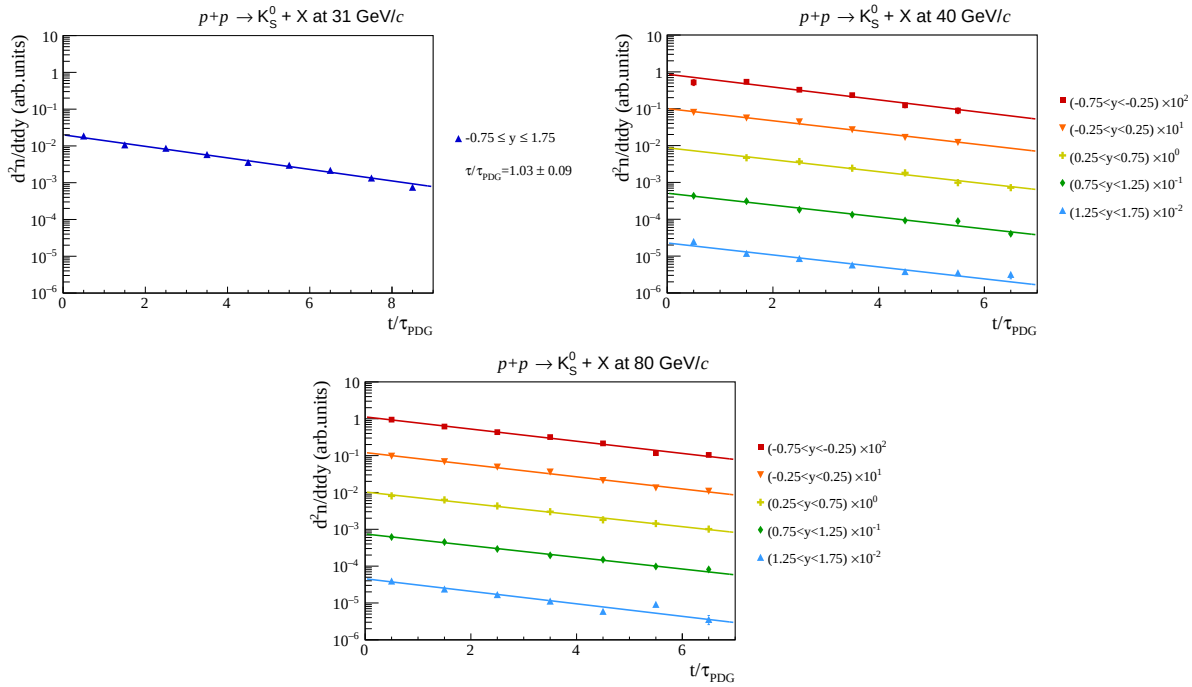

Figure 6: (Color online) Corrected lifetime distributions for K^0_S mesons produced in inelastic p+p interactions at beam energies of $p_{beam} = 31$ GeV/c (*top left*), $p_{beam} = 40$ GeV/c (*top right*), and $p_{beam} = 80$ GeV/c (*bottom*). The straight lines show the results of exponential fits used to obtain the mean lifetimes (normalized to the PDG value) in rapidity bins. Statistical uncertainties are smaller than the marker size and are not visible on the plots.

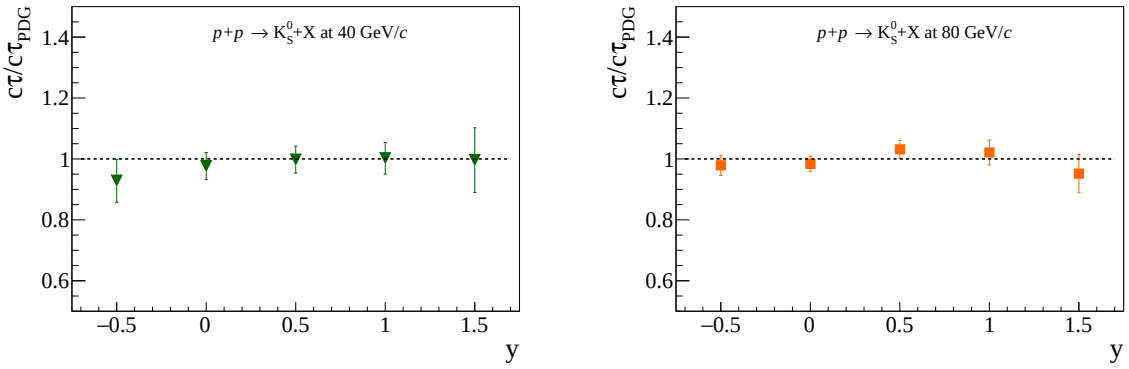

Figure 7: (Color online) Mean K^0_S lifetimes (normalized to the PDG value) obtained from fits to the lifetime distributions of Fig. 6 for the $p_{beam} = 40$ GeV/c (*left*) and $p_{beam} = 80$ GeV/c (*right*) data sets versus the rapidity y. The error bars indicate the statistical uncertainties.

4 Results

This section presents new NA61/SHINE results on inclusive K^0_S meson production from inelastic p+p interactions at beam momenta of 31, 40 and 80 GeV/c. Transverse momentum and rapidity spectra are obtained from the analysis of the weak decays of K^0_S mesons into two charged pions.

4.1 Transverse momentum spectra

Double differential K^0_S yields listed in Table 2 represent the main result of this paper. Yields are determined in five consecutive rapidity bins in the interval $-0.75 < y < 1.75$ and six transverse momentum bins in the interval $0.0 < p_T$ (GeV/c) < 1.2. The transverse momentum distributions at mid-rapidity ($y \approx 0$) are shown in Fig. 8.

An exponential function was fitted to the transverse momentum spectra. It reads:

$$f(p_T) = A \cdot p_T \cdot \exp\left(\frac{\sqrt{p_T^2 + m_0^2}}{T}\right) , \tag{10}$$

where m_0 is the mass of the K^0_S and T is the inverse slope parameter. The resulting values of T in each rapidity bin are listed in Table 3.

4.2 Rapidity distributions and mean multiplicities

Kaon yields in each rapidity bin were obtained from the measured transverse momentum distributions. The small fraction of K^0_S at high p_T outside of the acceptance was determined using Eq. 10. The resulting $\frac{dn}{dy}$ spectra of K^0_S mesons produced in inelastic p+p interactions at 31, 40 and 80 GeV/c are presented in Fig. 9 together with the previous NA61/SHINE results obtained for p+p interactions at 158 GeV/c [4].

Momentum		Results $\frac{d^2n}{dydp_T} \times 10^3$		
$p_{beam} = 31$ GeV/c	p_T (GeV/c) / y	(0.0;0.2)	(0.2;0.4)	(0.4;0.6)
	(-0.75;-0.25)	$19.2 \pm 5.1 \pm 6.6$	$44.6 \pm 8.8 \pm 7.0$	$35.9 \pm 8.0 \pm 11.7$
	(-0.25;0.25)	$24.5 \pm 3.4 \pm 4.4$	$56.1 \pm 4.6 \pm 3.9$	$40.7 \pm 3.4 \pm 2.6$
	(0.25;0.75)	$20.4 \pm 2.5 \pm 1.7$	$40.5 \pm 3.2 \pm 2.0$	$33.0 \pm 2.6 \pm 2.4$
	(0.75;1.25)	$15.7 \pm 2.4 \pm 4.6$	$21.7 \pm 2.5 \pm 1.9$	$21.7 \pm 2.3 \pm 2.1$
	(1.25;1.75)	$6.3 \pm 1.4 \pm 2.5$	$9.1 \pm 1.7 \pm 1.2$	$4.1 \pm 1.3 \pm 1.0$
	p_T (GeV/c) / y	(0.6;0.8)	(0.8;1.0)	(1.0;1.2)
	(-0.75;-0.25)	$13.3 \pm 3.6 \pm 3.8$	-	-
	(-0.25;0.25)	$18.7 \pm 2.0 \pm 1.6$	$10.2 \pm 1.2 \pm 1.6$	$4.2 \pm 0.8 \pm 0.7$
	(0.25;0.75)	$17.0 \pm 1.6 \pm 1.3$	$5.4 \pm 0.8 \pm 0.6$	$2.7 \pm 0.5 \pm 0.4$
	(0.75;1.25)	$7.6 \pm 1.2 \pm 0.5$	$2.3 \pm 0.6 \pm 0.7$	$1.2 \pm 0.4 \pm 0.2$
	(1.25;1.75)	$1.0 \pm 0.6 \pm 0.3$	-	-
$p_{beam} = 40$ GeV/c	p_T (GeV/c) / y	(0.0;0.2)	(0.2;0.4)	(0.4;0.6)
	(-0.75;-0.25)	$24.8 \pm 3.5 \pm 7.3$	$54.3 \pm 5.6 \pm 7.6$	$34.9 \pm 4.3 \pm 4.3$
	(-0.25;0.25)	$28.6 \pm 2.6 \pm 1.6$	$60.0 \pm 3.3 \pm 2.9$	$46.0 \pm 2.4 \pm 1.4$
	(0.25;0.75)	$26.5 \pm 2.0 \pm 2.4$	$51.1 \pm 2.7 \pm 2.8$	$38.1 \pm 2.2 \pm 2.6$
	(0.75;1.25)	$16.6 \pm 1.6 \pm 0.7$	$33.5 \pm 2.4 \pm 3.0$	$23.4 \pm 1.9 \pm 1.5$
	(1.25;1.75)	$9.4 \pm 1.2 \pm 1.1$	$13.6 \pm 1.9 \pm 2.6$	$8.7 \pm 1.5 \pm 1.3$
	p_T (GeV/c) / y	(0.6;0.8)	(0.8;1.0)	(1.0;1.2)
	(-0.75;-0.25)	$19.6 \pm 2.3 \pm 2.1$	$10.2 \pm 1.4 \pm 1.7$	$3.9 \pm 0.8 \pm 0.8$
	(-0.25;0.25)	$23.2 \pm 1.6 \pm 1.6$	$11.2 \pm 1.0 \pm 0.9$	$5.4 \pm 0.7 \pm 0.6$
	(0.25;0.75)	$22.1 \pm 1.4 \pm 1.8$	$8.7 \pm 0.9 \pm 1.2$	$3.2 \pm 0.5 \pm 0.4$
	(0.75;1.25)	$11.1 \pm 1.2 \pm 1.0$	$4.1 \pm 0.7 \pm 0.5$	$1.4 \pm 0.4 \pm 0.3$
	(1.25;1.75)	$5.2 \pm 1.2 \pm 2.3$	$0.9 \pm 0.5 \pm 0.2$	$0.3 \pm 0.2 \pm 0.1$
$p_{beam} = 80$ GeV/c	p_T (GeV/c) / y	(0.0;0.2)	(0.2;0.4)	(0.4;0.6)
	(-0.75;-0.25)	$35.2 \pm 2.5 \pm 3.5$	$64.2 \pm 2.9 \pm 2.6$	$51.8 \pm 2.4 \pm 2.9$
	(-0.25;0.25)	$35.0 \pm 2.0 \pm 2.1$	$68.6 \pm 2.5 \pm 2.0$	$63.8 \pm 2.2 \pm 1.9$
	(0.25;0.75)	$33.0 \pm 1.6 \pm 0.9$	$67.6 \pm 2.3 \pm 1.7$	$49.7 \pm 2.2 \pm 3.0$
	(0.75;1.25)	$23.6 \pm 1.3 \pm 1.0$	$50.8 \pm 2.0 \pm 1.6$	$35.3 \pm 2.1 \pm 1.7$
	(1.25;1.75)	$15.5 \pm 1.2 \pm 0.6$	$30.8 \pm 1.7 \pm 1.4$	$20.5 \pm 1.9 \pm 1.6$
	p_T (GeV/c) / y	(0.6;0.8)	(0.8;1.0)	(1.0;1.2)
	(-0.75;-0.25)	$28.0 \pm 1.6 \pm 1.7$	$13.4 \pm 1.0 \pm 0.6$	$5.6 \pm 0.7 \pm 0.5$
	(-0.25;0.25)	$31.6 \pm 1.5 \pm 1.9$	$15.4 \pm 1.0 \pm 1.1$	$6.4 \pm 0.6 \pm 0.5$
	(0.25;0.75)	$29.3 \pm 1.7 \pm 1.6$	$14.7 \pm 1.2 \pm 1.0$	$5.4 \pm 0.7 \pm 0.4$
	(0.75;1.25)	$22.0 \pm 2.0 \pm 1.3$	$7.4 \pm 1.3 \pm 0.9$	$3.4 \pm 0.9 \pm 0.3$
	(1.25;1.75)	$8.5 \pm 1.6 \pm 1.5$	$4.6 \pm 1.2 \pm 1.3$	$0.8 \pm 0.6 \pm 0.2$

Table 2: Double differential K^0_S yields in bins of (y, p_T). The first uncertainty is statistical, while the second one is systematic.

The mean multiplicities of K^0_S mesons were calculated as the sum of the measured data points in Fig. 9 scaled by the ratio between measured and unmeasured regions obtained from the Monte-Carlo simulation. The statistical uncertainties of $\langle K^0_S \rangle$ were calculated as the square root of the sum of the squares of the statistical uncertainties of the contributing bins. The systematic uncertainties were calculated as the square

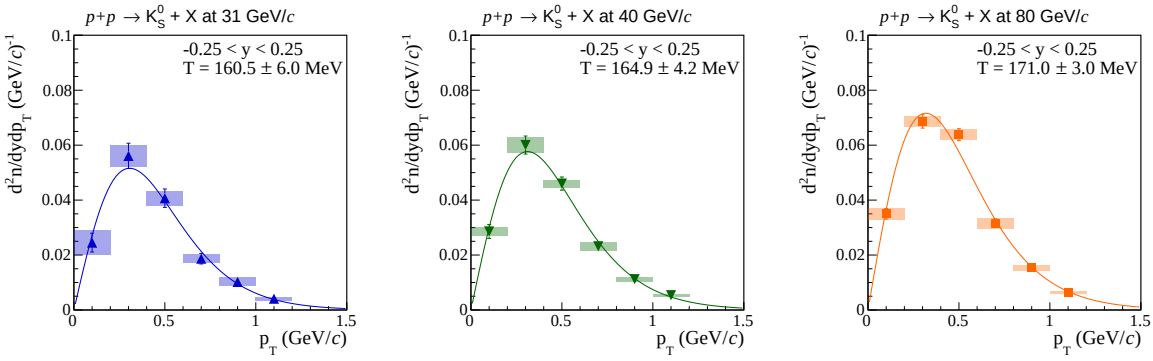

Figure 8: (Color online) Double-differential K^0_S spectra in inelastic p+p interaction at 31 GeV/c (*left*), 40 GeV/c (*middle*) and 80 GeV/c (*right*) at mid-rapidity ($y \approx 0$) calculated according to Eq. 4. Measured points are shown as blue full triangles up (for $p_{beam} = 31$ GeV/c), green full triangles down (for $p_{beam} = 40$ GeV/c) and orange full squares (for $p_{beam} = 80$ GeV/c). The solid curves are fitted to the data points using the exponential function (Eq. 10). Vertical bars indicate statistical uncertainties (for some points smaller than the symbol size). Shaded boxes show systematic uncertainties. Only statistical uncertainties are taken into account in the fit, because the systematic uncertainties do not depend on p_T. The numerical values of the data points are listed in Table 2.

	y	T (MeV)	$\frac{dn}{dy} \times 10^3$
$p_{beam} = 31$ GeV/c	(-0.75;-0.25)	$149.4 \pm 18.7 \pm 21.8$	$24.6 \pm 2.8 \pm 3.1$
	(-0.25;0.25)	$160.5 \pm 5.9 \pm 5.7$	$31.3 \pm 1.5 \pm 1.7$
	(0.25;0.75)	$152.5 \pm 4.9 \pm 3.7$	$24.1 \pm 1.1 \pm 1.0$
	(0.75;1.25)	$137.0 \pm 6.2 \pm 8.1$	$14.1 \pm 0.9 \pm 0.8$
	(1.25;1.75)	$93.5 \pm 11.7 \pm 11.2$	$4.2 \pm 0.6 \pm 0.8$
	y	T (MeV)	$\frac{dn}{dy} \times 10^3$
$p_{beam} = 40$ GeV/c	(-0.75;-0.25)	$162.6 \pm 6.8 \pm 9.7$	$30.0 \pm 1.7 \pm 2.6$
	(-0.25;0.25)	$164.8 \pm 4.2 \pm 1.9$	$35.5 \pm 1.0 \pm 1.4$
	(0.25;0.75)	$157.4 \pm 3.7 \pm 4.0$	$30.4 \pm 0.9 \pm 1.8$
	(0.75;1.25)	$143.6 \pm 4.5 \pm 2.6$	$18.2 \pm 0.8 \pm 1.0$
	(1.25;1.75)	$122.2 \pm 7.6 \pm 6.2$	$7.6 \pm 0.6 \pm 0.7$
	y	T (MeV)	$\frac{dn}{dy} \times 10^3$
$p_{beam} = 80$ GeV/c	(-0.75;-0.25)	$165.8 \pm 3.6 \pm 2.3$	$40.3 \pm 1.0 \pm 1.6$
	(-0.25;0.25)	$171.0 \pm 3.0 \pm 1.7$	$45.1 \pm 0.9 \pm 1.5$
	(0.25;0.75)	$168.0 \pm 3.4 \pm 2.4$	$40.7 \pm 0.8 \pm 1.2$
	(0.75;1.25)	$159.9 \pm 4.7 \pm 4.0$	$28.9 \pm 0.8 \pm 0.7$
	(1.25;1.75)	$140.6 \pm 6.2 \pm 3.9$	$16.2 \pm 0.7 \pm 0.7$

Table 3: Numerical values of T and dn/dy for K^0_S mesons produced in p+p interactions at 31, 40 and 80 GeV/c. The first column indicates the data set. The second column shows the rapidity range. The values of the inverse slope parameter are listed in the third column, along with their statistical and systematic uncertainties. The last column shows the numerical values of the p_T-integrated yields presented in Fig. 9 with statistical and systematic uncertainties.

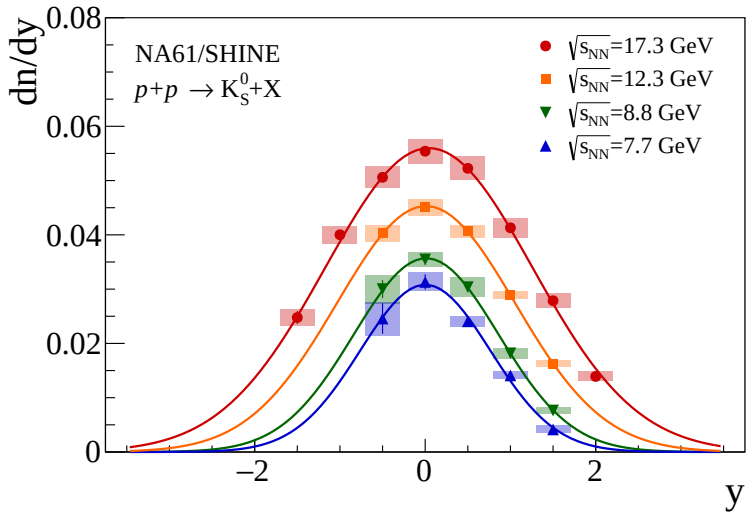

Figure 9: (Color online) Rapidity distribution dn/dy obtained by p_T-integration of data and extrapolation. Statistical uncertainties are shown by vertical bars (often smaller than the marker size), while shaded boxes indicate systematic uncertainties. The curves indicate the result of the Gaussian fit to the measured points. Points for p+p at $\sqrt{s_{NN}} =$ 17.3 GeV are taken from [4].

root of squares of systematic uncertainties described in Sec. 3.8. To estimate the systematic uncertainties of the method used to determine the mean multiplicities of K^0_S , the rapidity distributions were also fitted using a single Gaussian or two Gaussians symmetrically displaced from mid-rapidity. The deviations of the results of these fits from $\langle K^0_S \rangle$ are included as an additional contribution to the final systematic uncertainty. The mean multiplicities of K^0_S mesons in inelastic p+p collisions were found to be $0.0595 \pm 0.0019(stat) \pm 0.0022(sys)$ at 31 GeV/c, $0.0761 \pm 0.0013(stat) \pm 0.0031(sys)$ at 40 GeV/c and $0.1158 \pm 0.0012(stat) \pm 0.0037(sys)$ at 80 GeV/c.

5 Comparison with published world data and model calculations

This section compares the new NA61/SHINE measurements of K^0_S production in inelastic p+p interactions at 31, 40 and 80 GeV/c with world data as well as with microscopic model calculations (EPOS1.99 [16, 17], SMASH 2.0 [19] and PHSD [20, 21]). The K^0_S rapidity spectra from NA61/SHINE are compared in Fig. 10 to the results from Blobel *et al*. [22] as well as with results from Ammosov *et al*. [23]. The results from Blobel *et al*. at 24 GeV/c are significantly below the NA61/SHINE 31 GeV/c data in the central rapidity part. The results from Ammosov *et al*. at 69 GeV/c are located between the measured NA61/SHINE points of the 40 and 80 GeV/c data sets, as expected.

Recently NA61/SHINE reported an excess of charged over neutral kaon production in Ar+Sc collisions at 75A GeV/c [24]. The precise and detailed results on K^0_S production in p+p interactions reported here, together with the corresponding results on charged kaons [5], may contribute to the understanding of this puzzle. To this end the rapidity distributions of K^0_S are compared with two predictions derived from K^+ and K^- yields obtained from the same data sets [5]. The first prediction is based on valence- and sea-quark counting arguments [25] and leads to the equation $N_{K^0_S} = \frac{1}{4}(N_{K^+} + 3 \cdot N_{K^-})$. This relation was used in the

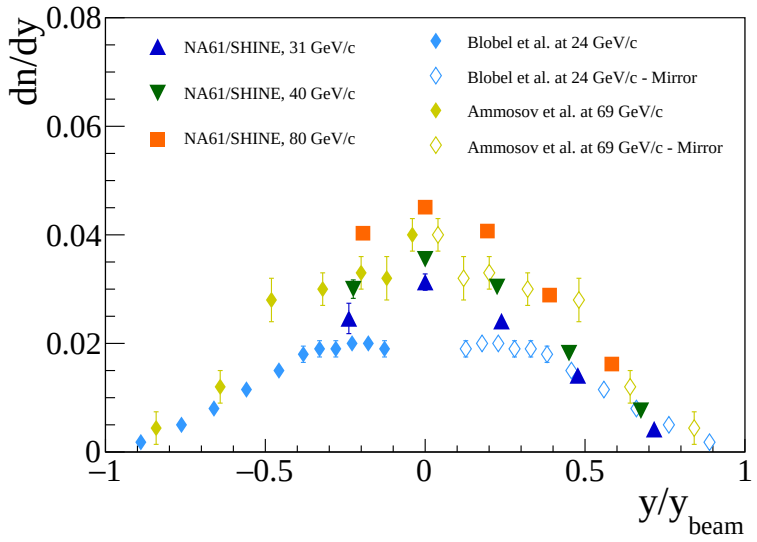

Figure 10: (Color online) dn/dy as a function of scaled rapidity y/y_{beam} of K^0_S mesons in inelastic p+p interactions at 31, 40 and 80 GeV/c. Measured points are shown as blue full triangles up (for $p_{beam} = 31$ GeV/c), green full triangles down (for $p_{beam} = 40$ GeV/c) and orange full squares (for $p_{beam} = 80$ GeV/c). Results from other experiments are shown as azure-colored diamonds (for Blobel *et al*. at 24 GeV/c) and yellow-colored diamonds (for Ammosov *et al*. at 69 GeV/c). Vertical bars indicate statistical uncertainties (for some points smaller than the symbol size).

past to estimate the neutral kaon flux in the fragmentation region for K^0 beam studies [26]. The second prediction assumes isospin symmetry of the different charge states of the kaon: $N_{K^0_S} = \frac{1}{2}(N_{K^+} + N_{K^-})$. The K^0_S rapidity distributions are compared to these two predictions in Fig. 11. The prediction based on valence quark counting describes the K^0_S rapidity distributions significantly better than the one assuming isospin symmetry.

Figure 12 compares the NA61/SHINE measurements with model calculations from EPOS1.99, PHSD and SMASH 2.0. EPOS1.99 overpredicts the experimental data at all three data beam momenta. PHSD overpredicts the measured $p_{beam} = 80$ GeV/c data, while for the remaining two data sets it shows fair agreement. SMASH 2.0 describes the experimental $p_{beam} = 80$ GeV/c data very well but underpredicts the remaining two data sets. All models exhibit the same shape of the rapidity distribution as the experimental data. The energy dependence of K^0_S production seems to be well reproduced by EPOS1.99, whereas PHSD and SMASH 2.0 both exhibit a stronger rise than observed in the data.

The mean multiplicity of K^0_S mesons in p+p collisions at $\sqrt{s_{NN}}$ = 7.7, 8.8, 12.3 GeV, reported here, and the published result at $\sqrt{s_{NN}} = 17.3$ GeV [4] are compared in Fig. 13 with the world data in the range from 3 - 32 GeV. The measured values are seen to rise linearly with collision energy $\sqrt{s_{NN}}$.

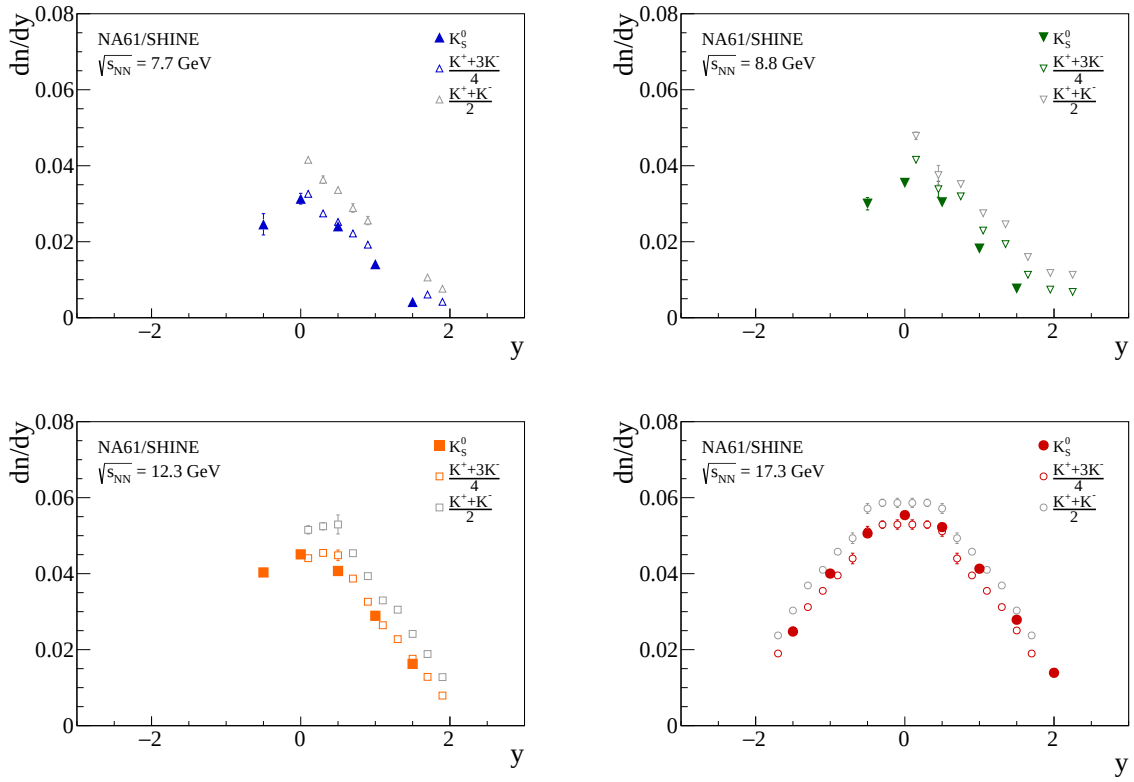

Figure 11: (Color online) Rapidity distribution dn/dy of K^0_S mesons in inelastic p+p interactions at 31, 40, 80 and 158 GeV/c. Measured points are shown as blue full triangles up for $p_{beam} = 31$ GeV/c (*top left*), green full triangles down for $p_{beam} = 40$ GeV/c (*top right*), orange full squares for $p_{beam} = 80$ GeV/c (*bottom left*) and red full circles for $p_{beam} = 158$ GeV/c (*bottom right*). Results for charged kaons obtained by formula $\frac{1}{4}(N_{K^+} + 3 \cdot N_{K^-})$ are shown by open colored symbols for all data sets, while the results obtained by formula $\frac{1}{2}(N_{K^+} + N_{K^-})$ are shown by grey opened symbols. Vertical bars indicate statistical uncertainties (for some points smaller than the symbol size).

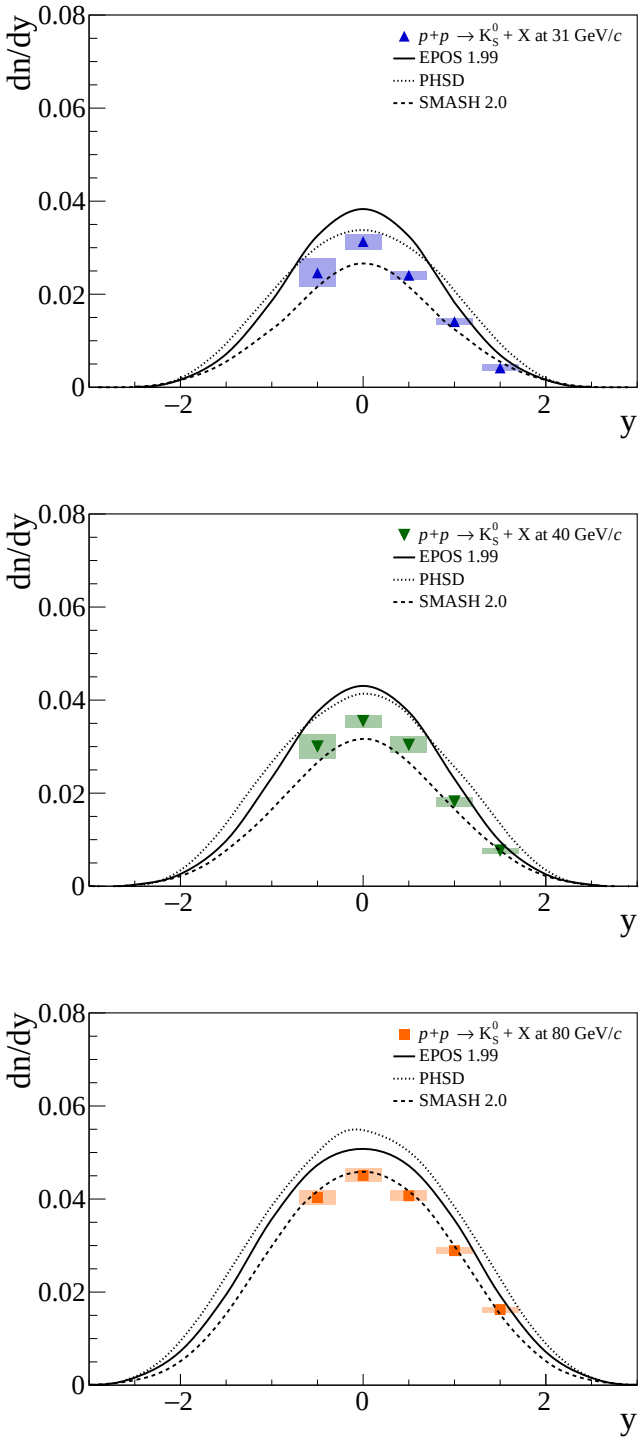

Figure 12: (Color online) Comparison of the experimental K^0_S rapidity distributions with model calculations. Colored symbols show the new measurements of NA61/SHINE as follows: $p_{beam} = 31$ GeV/c (*top*), $p_{beam} = 40$ GeV/c (*middle*) and $p_{beam} = 80$ GeV/c (*bottom*). The black curves show the result of the model calculations: EPOS1.99 (solid), PHSD (dotted) and SMASH 2.0 (dashed).

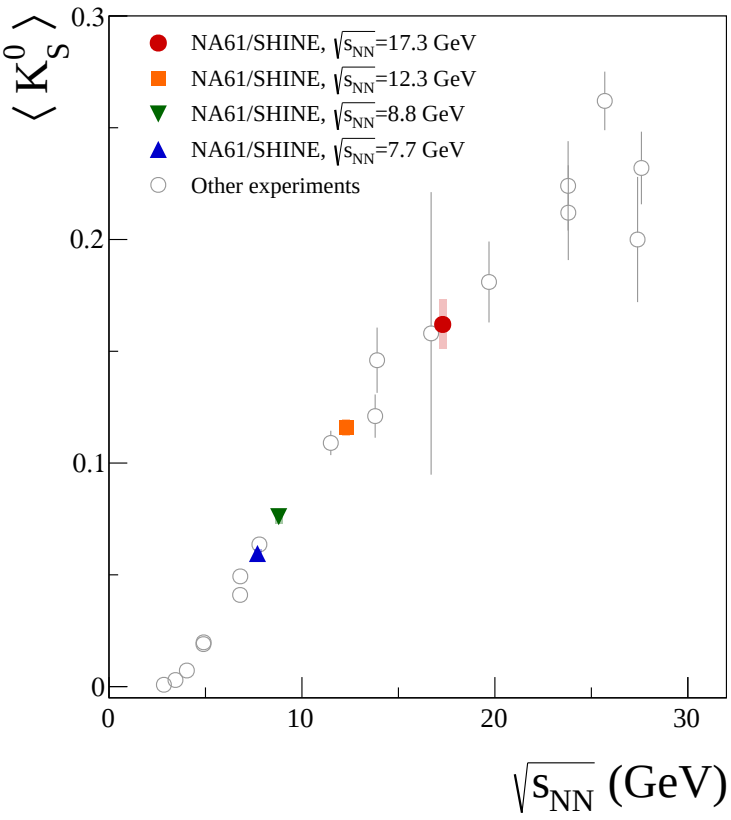

Figure 13: (Color online) Collision energy dependence of mean multiplicity of K^0_S mesons produced in p+p interactions. The measurements from NA61/SHINE are shown with colored symbols as follows: blue full triangle up for $p_{beam} = 31$ GeV/c, green full triangle down for $p_{beam} = 40$ GeV/c, orange full square for $p_{beam} = 80$ GeV/c and red full circle for $p_{beam} = 158$ GeV/c [4]. The results published by other experiments are shown by the grey open circles [22, 23, 27–40]. Statistical uncertainties are smaller than the marker size, while shaded boxes indicate systematic uncertainties.

6 Summary

This paper presents the new NA61/SHINE measurement of K^0_S mesons via their $\pi^+\pi^-$ decay mode in inelastic p+p collisions at beam momenta of 31, 40 and 80 GeV/c ($\sqrt{s_{NN}} = 7.7, 8.8$ and 17.3 GeV). Spectra of transverse momentum (up to 1.2 GeV/c), as well as a distributions of rapidity (from -0.75 to 1.75), are presented. The mean multiplicities, obtained from p_T-integrated spectra and extrapolated rapidity distributions, are $(5.95 \pm 0.19 \pm 0.22) \times 10^{-2}$ at 31 GeV/c, $(7.61 \pm 0.13 \pm 0.31) \times 10^{-2}$ at 40 GeV/c and $(11.58 \pm 0.12 \pm 0.37) \times 10^{-2}$ at 80 GeV/c, where the first uncertainty is statistical and the second systematic. The measured K^0_S lifetime agrees within uncertainties with the PDG value and thus confirms the quality of the analysis. The mean multiplicities from model calculations deviate by up to 10% from the measurements. The SMASH 2.0 model provides the best results for $p_{beam} = 31$ and 80 GeV/c, while the PHSD model has the best agreement with measured data for $p_{beam} = 40$ GeV/c. The results of K^0_S production in proton-proton interactions presented in this paper significantly improve, with their high statistical precision, the knowledge of strangeness production in elementary interactions and will serve as a reference for studies of strange hadron production in nucleus-nucleus collisions.

Acknowledgments

We would like to thank the CERN EP, BE, HSE and EN Departments for the strong support of NA61/SHINE.

This work was supported by the Hungarian Scientific Research Fund (grant NKFIH 138136/137812/138152 and TKP2021-NKTA-64), the Polish Ministry of Science and Higher Education (DIR/WK/2016/2017/10-1, WUT ID-UB), the National Science Centre Poland (grants 2014/14/E/ST2/00018, 2016/21/D/ST2/01983, 2017/25/N/ST2/02575, 2018/29/N/ST2/02595, 2018/30/A/ST2/00226, 2018/31/G/ST2/03910, 2020/39/O/ST2/00277), the Norwegian Financial Mechanism 2014–2021 (grant 2019/34/H/ST2/00585), the Polish Minister of Education and Science (contract No. 2021/WK/10), the European Union's Horizon 2020 research and innovation programme under grant agreement No. 871072, the Ministry of Education, Culture, Sports, Science and Technology, Japan, Grant-in-Aid for Scientific Research (grants 18071005, 19034011, 19740162, 20740160 and 20039012,22H04943), the German Research Foundation DFG (grants GA 1480/8-1 and project 426579465), the Bulgarian Ministry of Education and Science within the National Roadmap for Research Infrastructures 2020–2027, contract No. D01-374/18.12.2020, Serbian Ministry of Science, Technological Development and Innovation (grant OI171002), Swiss Nationalfonds Foundation (grant 200020117913/1), ETH Research Grant TH-01 07-3, National Science Foundation grant PHY-2013228 and the Fermi National Accelerator Laboratory (Fermilab), a U.S. Department of Energy, Office of Science, HEP User Facility managed by Fermi Research Alliance, LLC (FRA), acting under Contract No. DE-AC02-07CH11359 and the IN2P3-CNRS (France).

The data used in this paper were collected before February 2022.

References

[1] J. Letessier and J. Rafelski, *Hadrons and Quark–Gluon Plasma*. Oxford University Press, 2002.

[2] M. Gazdzicki and M. I. Gorenstein, "On the early stage of nucleus-nucleus collisions," *Acta Phys. Polon.* **B30** (1999) 2705, arXiv:hep-ph/9803462 [hep-ph].

[3] M. Gazdzicki, Z. Fodor, and G. Vesztergombi, [NA49-future Collaboration Collab.], "Study of Hadron Production in Hadron-Nucleus and Nucleus-Nucleus Collisions at the CERN SPS," Tech. Rep. CERN-SPSC-2006-034. SPSC-P-330, CERN, Geneva, Nov, 2006. https://cds.cern.ch/record/995681. revised version submitted on 2006-11-06 12:38:20.

[4] A. Acharya *et al.*, [NA61/SHINE Collab.], "K^0_S meson production in inelastic p+p interactions at 158 GeV $/c$ beam momentum measured by NA61/SHINE at the CERN SPS," *Eur. Phys. J. C* **82** no. 1, (2022) 96, arXiv:2106.07535 [hep-ex].

[5] A. Aduszkiewicz *et al.*, [NA61/SHINE Collab.], "Measurements of $\pi^{\pm}$, $\mathrm{K}^{\pm}$, p and $\bar{\mathrm{p}}$ spectra in proton-proton interactions at 20, 31, 40, 80 and 158 GeV$/c$ with the NA61/SHINE spectrometer at the CERN SPS," *Eur. Phys. J. C* **77** no. 10, (2017) 671, arXiv:1705.02467 [nucl-ex].

[6] N. Abgrall *et al.*, [NA61 Collab.], "NA61/SHINE facility at the CERN SPS: beams and detector system," *JINST* **9** (2014) P06005, arXiv:1401.4699 [physics.ins-det].

[7] N. Abgrall *et al.*, [NA61/SHINE Collab.], "Measurement of negatively charged pion spectra in inelastic p+p interactions at p_{lab} = 20, 31, 40, 80 and 158 GeV/c," *Eur. Phys. J. C* **74** no. 3, (2014) 2794, arXiv:1310.2417 [hep-ex].

[8] A. Aduszkiewicz *et al.*, [NA61/SHINE Collab.], "Multiplicity and transverse momentum fluctuations in inelastic proton–proton interactions at the CERN Super Proton Synchrotron," *Eur. Phys. J. C* **76** no. 11, (2016) 635, arXiv:1510.00163 [hep-ex].

[9] A. P. C. Bovet, R. Maleyran and M. Placidi, "The cedar (cerenkov differential counters with achromatic ring focus) project," *IEEE Transactions on Nuclear Science* **25** no. 1, (1978) 572–576.

[10] C. Strabel, *Evaluation of Particle Yields in 30 GeV Proton-Carbon Inelastic Interactions for Estimating the T2K Neutrino Flux*. PhD thesis, Frankfurt U., 2011.

[11] A. Aduszkiewicz *et al.*, [NA61/SHINE Collab.], "Two-particle correlations in azimuthal angle and pseudorapidity in inelastic p + p interactions at the CERN Super Proton Synchrotron," *Eur. Phys. J. C* **77** no. 2, (2017) 59, arXiv:1610.00482 [nucl-ex].

[12] N. Abgrall, [NA61 Collab.], "Calibration and Analysis of the 2007 Data," tech. rep., CERN, Geneva, 2008. https://cds.cern.ch/record/1113279.

[13] M. Tanabashi *et al.*, [Particle Data Group Collab.], "Review of Particle Physics," *Phys. Rev. D* **98** no. 3, (2018) 030001.

[14] A. Aduszkiewicz *et al.*, [NA61/SHINE Collab.], "$K^*(892)^0$ meson production in inelastic p+p interactions at 158 GeV/c beam momentum measured by NA61/SHINE at the CERN SPS," *Eur. Phys. J. C* **80** no. 5, (2020) 460, arXiv:2001.05370 [nucl-ex].

[15] J. Podolanski and R. Armenteros, "III. Analysis of V-events," *The London, Edinburgh, and Dublin Philosophical Magazine and Journal of Science* **45** no. 360, (1954) 13–30. https://doi.org/10.1080/14786440108520416.

[16] K. Werner, F. M. Liu, and T. Pierog, "Parton ladder splitting and the rapidity dependence of transverse momentum spectra in deuteron-gold collisions at RHIC," *Phys. Rev. C* **74** (2006) .

[17] T. Pierog and K. Werner, "EPOS Model and Ultra High Energy Cosmic Rays," *Nucl. Phys. B Proc.* **196** (2009) 102–105.

[18] R. Brun *et al.*, *GEANT: Detector Description and Simulation Tool; Oct 1994*. CERN, Geneva, 1993. https://cds.cern.ch/record/1082634. Long Writeup W5013.

[19] J. Mohs, S. Ryu, and H. Elfner, "Particle Production via Strings and Baryon Stopping within a Hadronic Transport Approach," *J. Phys. G* **47** no. 6, (2020) 065101, arXiv:1909.05586 [nucl-th].

[20] W. Cassing and E. L. Bratkovskaya, "Parton transport and hadronization from the dynamical quasiparticle point of view," *Phys. Rev. C* **78** (2008) 034919, arXiv:0808.0022 [hep-ph].

[21] W. Cassing and E. L. Bratkovskaya, "Parton-Hadron-String Dynamics: an off-shell transport approach for relativistic energies," *Nucl. Phys. A* **831** (2009) 215–242, arXiv:0907.5331 [nucl-th].

[22] V. Blobel *et al.*, "Multiplicities, topological cross sections, and single particle inclusive distributions from pp interactions at 12 and 24 GeV/c," *Nuclear Physics B* **69** (1974) 454–492.

[23] V. V. Ammosov *et al.*, "Neutral Strange Particle Production in p p Interactions at 69-GeV/c," *Nucl. Phys. B* **115** (1976) 269–286.

[24] H. Adhikary, [NA61 Collab.], "Excess of charged over neutral K meson production in high-energy collisions of atomic nuclei," tech. rep., CERN, Geneva, 2023. arXiv:2312.06572. https://cds.cern.ch/record/2883229. 18 pages, 6 figures.

[25] J. Stepaniak and D. Pszczel, "On the relation between K^0_s and charged kaon yields in proton–proton collisions," *Eur. Phys. J. C* **83** no. 10, (2023) 928, arXiv:2305.03872 [hep-ph].

[26] L. Gatignon, "Design and Tuning of Secondary Beamlines in the CERN North and East Areas,". https://cds.cern.ch/record/2730780.

[27] R. I. Louttit, T. W. Morris, D. C. Rahm, R. R. Rau, A. M. Thorndike, W. J. Willis, and R. M. Lea, "Production of strange particles in $p-p$ collisions at 2.85 GeV," *Phys. Rev.* **123** (Aug, 1961) 1465–1471. https://link.aps.org/doi/10.1103/PhysRev.123.1465.

[28] G. Alexander *et al.*, "Proton-Proton Interactions at 5.5 GeV/c," *Phys. Rev.* **154** (1967) 1284–1304.

[29] M. Firebaugh *et al.*, "Strange-particle production in 8-GeV/c proton-proton interactions," *Phys. Rev.* **172** (1968) 1354–1369.

[30] H. Fesefeldt *et al.*, "Strangeness-transfer distributions in proton-proton collisions at 12 and 24 GeV/c," *Nuclear Physics B* **147** (1979) 317–335.

[31] M. Y. Bogolyubsky *et al.*, "Study of Neutral Strange Particle Production in pp Interactions at 32-GeV/c and Comparison With $\bar{p}p$ Data," *Sov. J. Nucl. Phys.* **50** (1989) 424.

[32] M. Alston-Garnjost *et al.*, "Neutral particle production in $\pi^+ p$ and pp collisions at 100 GeV/c," *Phys. Rev. Lett.* **35** (Jul, 1975) 142–145.

[33] J. W. Chapman *et al.*, "Production of γ, Λ^0, K^0_S and $\bar{\Lambda^0}$ in pp collisions at 102 GeV/c," *Physics Letters B* **47** (1973) 465–468.

[34] D. Brick *et al.*, "Inclusive production of neutral strange particles by 147-GeV/c Pi+ K+ p interactions in hydrogen," *Nucl. Phys. B* **164** (1980) .

[35] K. Jaeger *et al.*, "Characteristics of V^0 and γ production in pp interactions at 205 GeV/c," *Phys. Rev. D* **11** (May, 1975) 2405–2425.

[36] A. Sheng *et al.*, "pp interactions at 300 GeV/c: γ and neutral-strange-particle production," *Phys. Rev. D* **11** (Apr, 1975) 1733–1742.

[37] F. LoPinto *et al.*, "Inclusive K^0, Λ^0, $K^{*\pm}(890)$, and $\Sigma^{*\pm}(1385)$ production in pp collisions at 300 GeV/c," *Phys. Rev. D* **22** (Aug, 1980) 573–581.

[38] M. Asai *et al.*, [EHS-RCBC, Bombay-CERN-Genoa-Innsbruck-Japan-Madrid-Mons-Rutgers-Serpukhov-Tennessee-Vienna Collab.], "Inclusive K^0_S, Λ and $\bar{\Lambda}$ Production in 360-GeV/cpp Interactions Using the European Hybrid Spectrometer," *Z. Phys. C* **27** (1985) 11.

[39] R. D. Kass *et al.*, "Charged- and neutral-particle production from 400-GeV/c pp collisions," *Phys. Rev. D* **20** (Aug, 1979) 605–614.

[40] H. Kichimi *et al.*, "Inclusive study of strange-particle production in pp interactions at 405 GeV/c," *Phys. Rev. D* **20** (Jul, 1979) 37–52.